Sensing performance of SnO$_2$ film fabricated by sputtering deposition

N. M. Shaalan[1,2] · M. Rashad[2,3] · T. Yamazaki[1]

Abstract The effects of in situ-deposition temperature and post-deposition annealing on the microstructure of the sputtered SnO$_2$ thin film are studied. These effects on the performance of the resulting gas-sensing devices have been characterized. For in situ-deposition temperature, the film was deposited on a heated substrate, while for post-deposition annealing, the film was deposited on an unheated substrate and then annealed it at various temperatures. Microstructure changes in SnO$_2$ film were induced at various temperatures. Both films of in situ heating and post-annealing evoked only partial crystallization, especially at low temperatures, and the crystallinity was enhanced with high temperatures. SEM images confirmed that the grains and pores of the film changed with the thermal treatment. In consequence of the post-annealing, the pores grew wider; however, they grew narrow in the case of in situ heating. The film annealed at low temperature yielded high-response device to NO$_2$ gas compared with that annealed at higher temperature. The sensing devices fabricated by in situ deposition showed highest response.

✉ N. M. Shaalan
  nshaalan@aun.edu.eg

✉ M. Rashad
  mohamed.ahemed24@sceince.au.edu.eg

  T. Yamazaki
  yamazaki@eng.u-toyama.ac.jp

[1] Graduate School of Science and Engineering, University of Toyama, 3190 Gofuku, Toyama 930-8555, Japan

[2] Department of Physics, Faculty of Science, University of Assiut, Assiut 71516, Egypt

[3] Department of Physics, Faculty of Science, University of Tabuk, P.O. Box 741, Tabuk 71491, KSA

1 Introduction

Nitrogen dioxide (NO$_2$), which is the most common oxide of nitrogen, is toxic, highly reactive oxidant, and corrosive gas. The most important sources of NO$_2$ are internal combustion engines, thermal power stations, etc. [1], as known that NO$_2$ causes an impairing in the lung function and respiratory system with long-term exposure [2]. Therefore, it is essential to develop a high-performance sensor for easily detecting NO$_2$ gas. Gas sensors made of oxide semiconductors have been widely used as domestic and industrial gas sensors because of their high sensitivity, quick response, and low cost [3]. However, most of these gas sensors are operable at a high temperature of a sensing element of above 200 °C, which results in high power consumption and complexity in the integration [4–9]. Therefore, most researchers have focused their attention on the sensing material to improve the sensing properties [10–12], and some researchers have focused on the effect of electrode material and geometry on the sensing properties [13–15].

Advanced oxidation processes in the presence of semiconductor and metal oxide have received important attention in the last decade for gas sensor application. There is a considerable interest in tin oxide (SnO$_2$) as one of the most promising n-type semiconductor material for different applications because of its physical, chemical properties and effective cost [16–18]. SnO$_2$ film is used in many applications, such as gas sensor [19] and transparent electrode [16]. Several chemical and physical methods, such as sol–gel [20], ultrasonic spray pyrolysis [21], chemical vapor deposition [22], pulsed laser deposition [23], and sputtering [24], have been used to prepare SnO$_2$ film. Among them, the reactive sputtering deposition has shown the advantages of controlling the crystalline orientation,

growing temperatures, interfacial adhesion to the substrate, and density of the grown film. However, the thermal treatment process to stabilize or improve the operation performance of gas sensor sometimes is required for amorphous thin films deposited by sputtering technique. The thermal treatment leads to the change in the microstructure factors, such as crystallite size, pore size distribution, density of adsorption sites and the density of the film. Consequently, the control and the effect of microstructure possess the attention to control and improve the performance of the sensing material of oxide [25–27].

According to our knowledge, many experimental and theoretical studies have been performed and reviewed for SnO_2 thin film [28–30]. However, the interest in the present study is the influence of in situ heating and post-annealing on the surface morphology and NO_2 sensing properties of sensor fabricated by using sputtering technique. The effect of the synthesis conditions on the specific surface area, and pore structure of DC sputtering thin film which is to be used to make gas sensor are investigated. The sensing property is carried out for the SnO_2 sensor to NO_2 gas at various surface temperatures as well as NO_2 concentrations.

2 Experimental details

2.1 Preparations of SnO_2 film

A film with a thickness of 100 nm was deposited on oxidized silicon substrate by reactive DC magnetron sputtering using a circular tin target with a diameter of 100 mm. The purity of the tin target was 99.99 %. After the sputtering chamber was evacuated to a background pressure below 2×10^{-4} Pa, the chamber was maintained at mixture gas of air and O_2 with a ratio of 1:1, and discharge gas pressure of 20 Pa, and then the SnO_2 film was reactively deposited at a DC input power of 17 Watt with a deposition rate of 1 nm/min. For post-annealing, the film was firstly deposited and then annealed for 1 h in ambient air at temperature of 350, 500, and 650 °C. For in situ heating, the substrate was maintained at temperature of 200, 350, and 500 °C, and then SnO_2 film was deposited. Before the deposition, the target was pre-sputtered for 5 min with controlling a moveable shutter placed between the target and substrate.

2.2 Characterization of SnO_2 film

The crystallographic structure of the sputtered film was investigated by X-ray diffraction (XRD) using an X-ray diffractometer (Shimadzu XRD-6100) with Cu Kα source in the range of $2\theta = 15°–65°$. The morphology was

observed by field emission scanning electron microscope (FESEM) (JEOL JSM-6700F). Pore surface area and pore size distribution were determined by using argon gas and the adsorption–desorption method described in Refs. [31, 32]. For the measurement of the physical adsorption isotherms, the film was deposited on the front and rear surfaces of 4-in Si wafer, both sides of the wafer were mirror-polished and oxidized. About 50 strips with a size of 25×5 mm^2 were cut out of the wafer and introduced into the sample cell of the physical adsorption apparatus.

2.3 Gas-sensing properties of SnO_2 film

For investigation of NO_2 gas-sensing properties, SnO_2 film of 100 nm thick was deposited on a pair of inter-digitated Pt electrodes which have a thickness of 100 nm, an area of 25 mm^2, and a gap size of 20 μm, as shown in the scheme of Fig. 1. The sensors were placed in a quartz tube, which was inserted into an electric furnace. The operating temperature was varied from RT to 300 °C. Dry synthetic air, mixed with NO_2 gas, was passed at a rate of 200 ml/min. It was possible with a computer-controlled measurement system to control both temperature and gas atmosphere in the measurement chamber during the operations. In order to have comparable results, the samples were measured at the same conditions so that the environment and the state of the semiconductor surface would be the same. Moreover, the measurements of gas sensing were made twice at long interval in order to monitor the reproducibility and stability of the sensor. The sensor response (S) was defined by $S = (R_g - R_a)/R_a$, where R_a is the resistance in the air, and R_g is the resistance after introduction of gas.
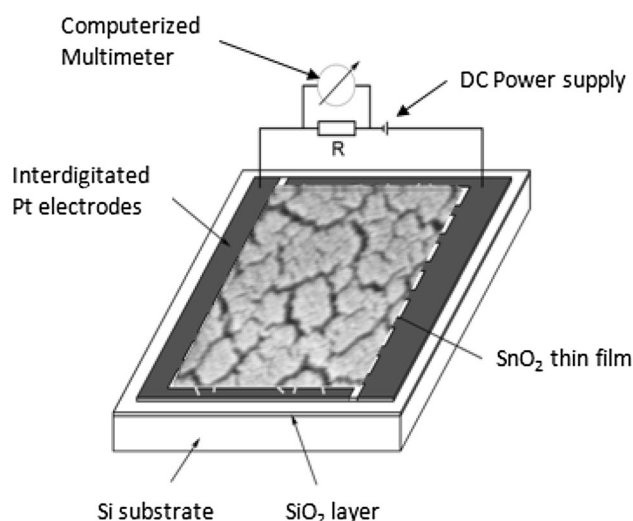

Fig. 1 Illustration of SnO_2 sensor diagram

3 Results and discussions

3.1 Microstructure characteristics

Typical XRD patterns recorded for the SnO_2 film are shown in Fig. 2. For as-deposited film, the film is mainly amorphous with a broadening peak observed around 33°. The post-annealing temperature of 350 °C is somewhat sufficient for partial crystallization of SnO_2, as shown from the peaks observed in 26.32°, 34.02°, and 61.75°. These peak intensities increased when the annealing temperature increased up to 500 °C. The same peaks for a high temperature of 650 °C film are observed with a slight increase in the intensity. These peaks were indexed on a tetragonal structure (JCPDS No. 21-1250) of SnO_2 for (110), (101), (211), and (310) planes. The as-deposited and post-annealed films are partially crystallized, as known that the energy required for crystallization is related to the melting point of the formed material. The partial crystallization can be induced at low temperature if the in situ heating is applied to the substrate during the deposition. This can be seen in Fig. 3. From XRD charts of in situ heating, the change in the crystallinity of film with the temperature is hardly observed, comparing with that of post-annealing.

In the in situ-heated film, the temperature during deposition causes the surface atoms just landed not to be frozen in at their landing sites, but diffuse by the available thermal energy on the surface of substrate. Thus, the aggregations of nanocrystals are due to the thermal energy of the substrate surface, where surface adatom mobility occurs in each atomic layer during the deposition and it is dictated by the heating during the deposition [33]. As a consequence of the adatom mobility, there is in each layer an atomic environment which is sufficiently close to the crystalline SnO_2. Therefore, moderate deposition temperatures are
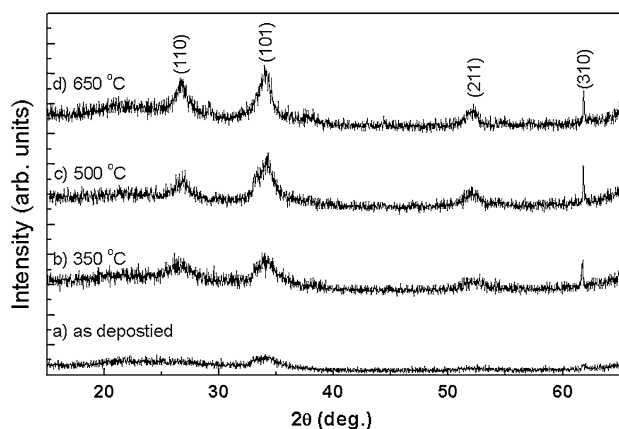

Fig. 2 XRD of SnO₂ film on Si(100) substrate: as-deposited and post-deposition annealed film
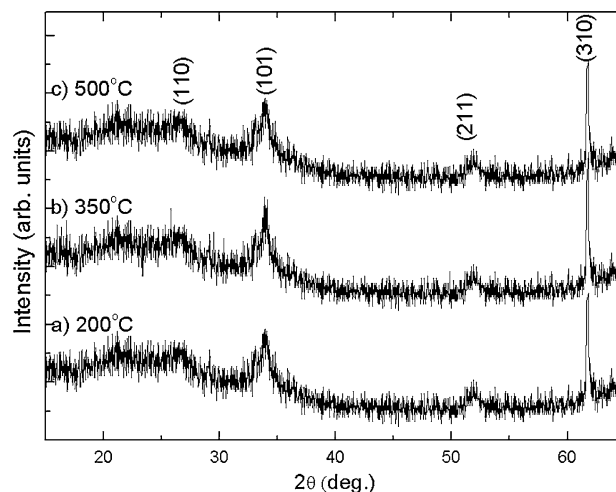

Fig. 3 XRD of SnO₂ film on Si(100) substrate: the in situ-deposition heated film

sufficient for partial crystallization. Unlike in the case of a deposition at unheated substrate, atoms arrive and settle at their landing locations with limited mobility for rearrangement for crystal formation and only short-range ordering might exist. This situation is happening in each layer and when the process of deposition is stopped, the structure remains frozen in. Therefore, high temperatures will be required to rearrange the atoms to the required crystalline formation.

The FESEM images of SnO_2 film are shown in Fig. 4. Both of the in situ-heated and post-annealed films are composed of grains and pores. The grains contact with each other through the necks, and pores are observed throughout the film. At post-annealing temperature of 350 °C, the partial crystallization of the film affected the grain size, grain contacts, and pore size, as shown in Fig. 4a. The average grain size of the film annealed at low temperatures of 350 °C was ∼50 nm. The grains as well as the pores grew up when the post-annealing temperature raised up to 500 °C. Large grains can be seen at a high temperature of 650 °C, and accompanied large pores can be also seen, indicating the development of pore size during the annealing. The formation of large pores is owing to the porosity and the low density of the as-deposited film due to the high discharge pressure of 20 Pa [30, 34]. Unlike in the case of in situ-heating treatment, the small grains surrounded by short pores are observed at low temperature of 200 °C. The grains grew larger and are surrounded with few large pores at a substrate temperature of 350 °C. The film became denser, and the grain boundaries can be lightly seen where the pores reduced to a very small size. However, when the density of the film was measured, it was much lower than that of a tin oxide bulk, indicating that the film is still porous.
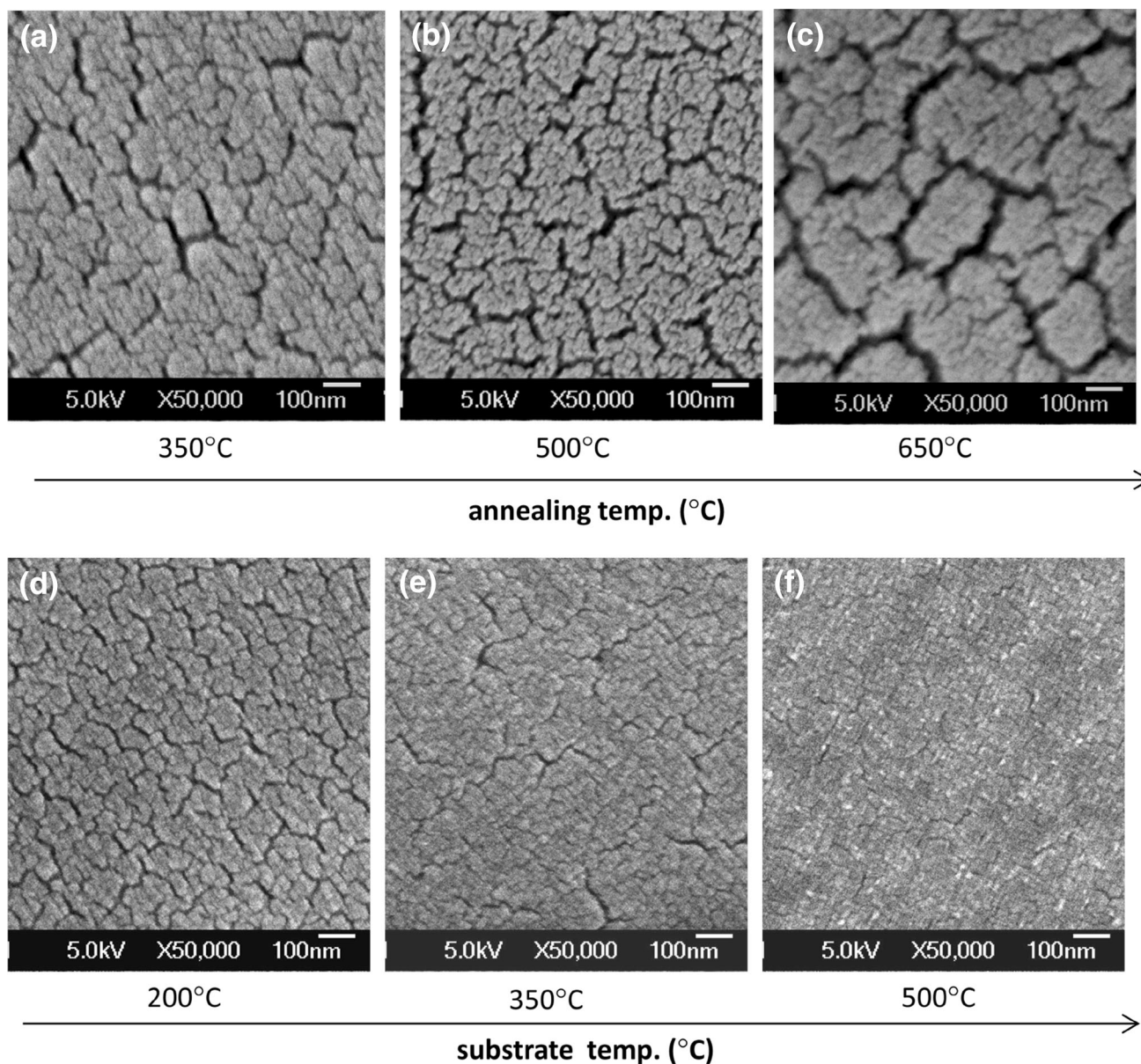
Fig. 4 FESEM images of SnO$_2$ film: **a–c** post-deposition annealed film, and **d–f** film deposited on a heated substrate

For deeper understanding the pore size distribution of SnO$_2$ film, the pore size distribution was measured by the physical adsorption–desorption method. Barrett–Joyner–Halenda (BJH) method was used to calculate the total pore volume and pore surface area which were measured by using argon gas. The pore size distribution of the in situ-heated and post-annealed film is shown in Fig. 5. In the post-annealed film, the pores of the film annealed at 350 °C are mostly distributed in the range of 1.5–10.0 nm and have a peak at 2.7 nm which corresponds to a specific area of ∼380 cm^2/g. The pores of the film annealed at 500 °C are distributed in the range of 2.0–6.5 nm and have a peak at 2.7 nm which corresponds to a specific area of ∼315 cm^2/g. One can also see that the film annealed at

650 °C shows a pore size distribution between small size of 1.8–3.0 nm and large size of 10–15 nm with peaks at 2 and 13 nm and specific areas of 210 and 45 cm^2/g, respectively. The result of the post-annealing samples indicated that although the pores exceeded, the specific area reduced. The samples prepared on heated substrates have pores distributed in the range of 0.6–25.0, 0.6–15.0, and 0.6–7.0 nm for the film deposited at 200, 350, and 500 °C, respectively. In the later films, the pore distributed in the range of 0.6–5 nm is dominated and has large specific area. The range of pore distribution of in situ-deposition film is wider than that of post-annealing film. The pore size distribution, specific area of the peaks, and total pore volume are shown in Table 1. The total pore volume of the
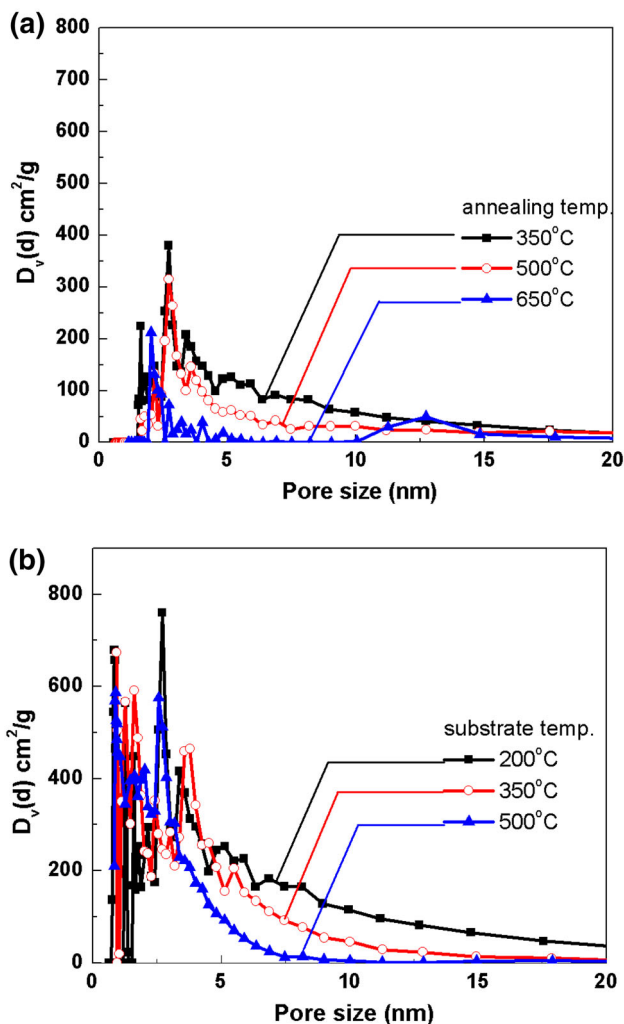
Fig. 6 Total pore volume measured for in situ- and post-deposition annealed film

Fig. 5 Pore size distribution of porous SnO$_2$ film: **a** post-deposition annealed film and **b** film deposited on a heated substrate

heated substrate. According to the context of physisorption reports, the pores observed in the present film are classified as mesopores [32].

3.2 NO$_2$ gas-sensing characteristics

The signal of SnO$_2$ sensors upon exposure to different concentrations of NO$_2$ gas at operating temperature of 150 °C is shown in Fig. 7. The resistance increased to a steady value when the sensor was exposed to NO$_2$ gas and then decreased when the gas was switched off. The resistance further increased as the sensors are being exposed to more concentration of NO$_2$. This indicates that NO$_2$ undergoes a reversible oxidizing interaction with the tin oxide surface. The change in resistance with concentration is remarkably observed in the resistance of a post-annealed sensor than in the in situ-heated sensors. Generally, the adsorbed layer of gas left the surface of oxide soon after the end of gas exposure, bringing the sensor signal back approximately to its baseline, indicating a good reversibility of these sensors. The very similar response to

corresponding film is also presented in Fig. 6. The in situ- and post-deposition treatment caused a reduction in the total pore volume. The total pore volume of the post-annealed film is dramatically reduced at high temperatures, whereas it was slightly reduced for the film deposited on
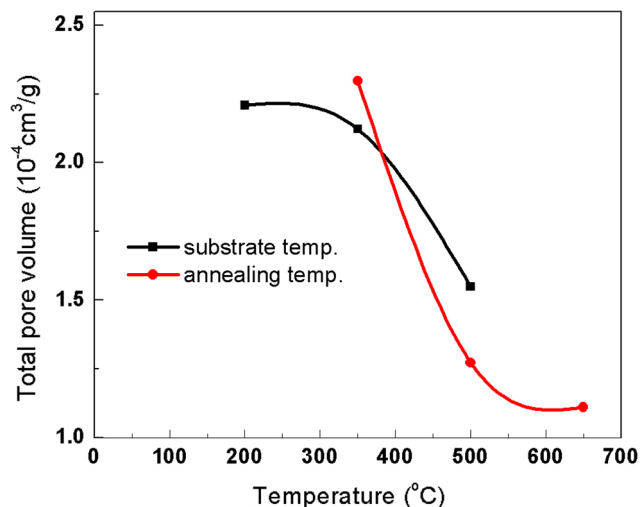
Table 1 Pore size distribution, specific area, and total pore volume versus temperatures

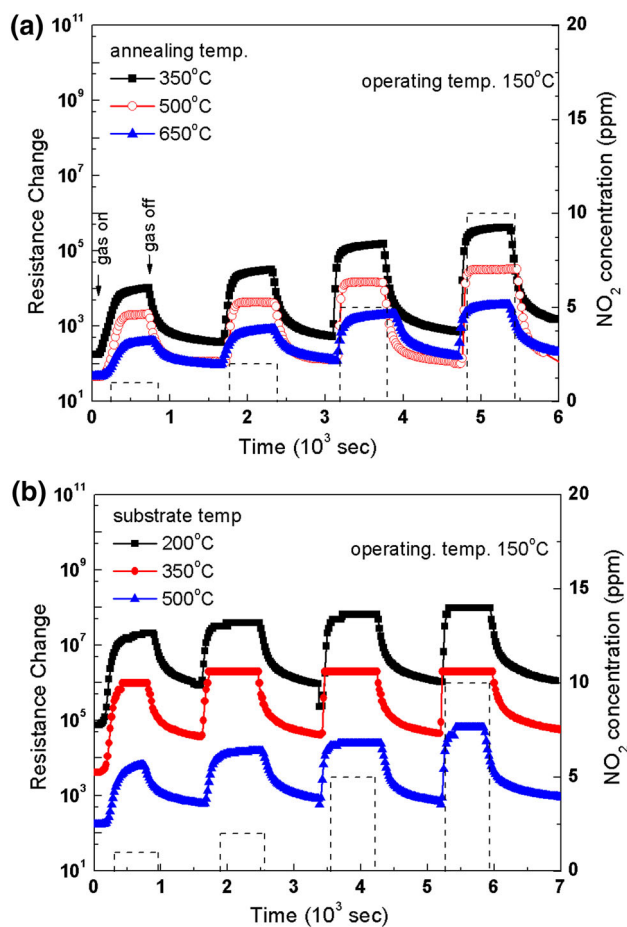| Temp. (°C)	Pore size distribution range (nm)	Peak at (nm)/specific area (cm^2/g)	Total pore volume (10^{-4} cm^3/g)
Post-deposition thermal treatment			
350	1.5–10.0	2.7/380	2.298
500	2.0–6.5	2.7/315	1.273
650	1.8–3, 10.0–15.0	2.0/210, 13.0/45	1.110
In situ-deposition thermal treatment			
200	0.6–25.0	0.9/670, 1.5/455, 2.7/760, 3.5/414	2.209
350	0.6–15.0	0.9/670, 1.3/566, 1.5/583, 3.6/466	2.122
500	0.6–7.0	0.9/583, 1.7/417, 2.5/572	1.549

Fig. 7 Change in resistance versus the time at different concentrations of NO_2 at operating temperature of 150 °C

Fig. 8 Response of sensors at different operating temperatures. *Note* the dotted curve obtained by a smooth fitting is only guide for the eye

sequential gas pulse of the same concentrations showed a high reproducibility of the sensor response. Remarkably, very little baseline drift has occurred after the final concentration of NO_2 had been reached. It was reported that this small drift occurs due to the poison reaction on the surface of tin oxide [28], when the sensor takes more time to return to its baseline.

The response of sensors upon exposure to 2 ppm concentration at various operating temperatures is shown in Fig. 8. For post-annealed sensor, the sensor is slightly sensitive for NO_2 at low operating temperatures, and its response increased with operating temperature. The sensor became highly sensitive at operating temperature of 100 °C, and it became again less sensitive at higher temperatures. The peak response observed in the post-annealed sensor is 338, 213, and 24 for annealing temperatures of 350, 500, and 650 °C, respectively. With increasing the annealing temperature up to 500 °C, the response slightly decreased, while drastically decreased at 650 °C, as shown in Fig. 8a. The similar behavior of operating temperature dependence of the response curve for post-annealed sensors was
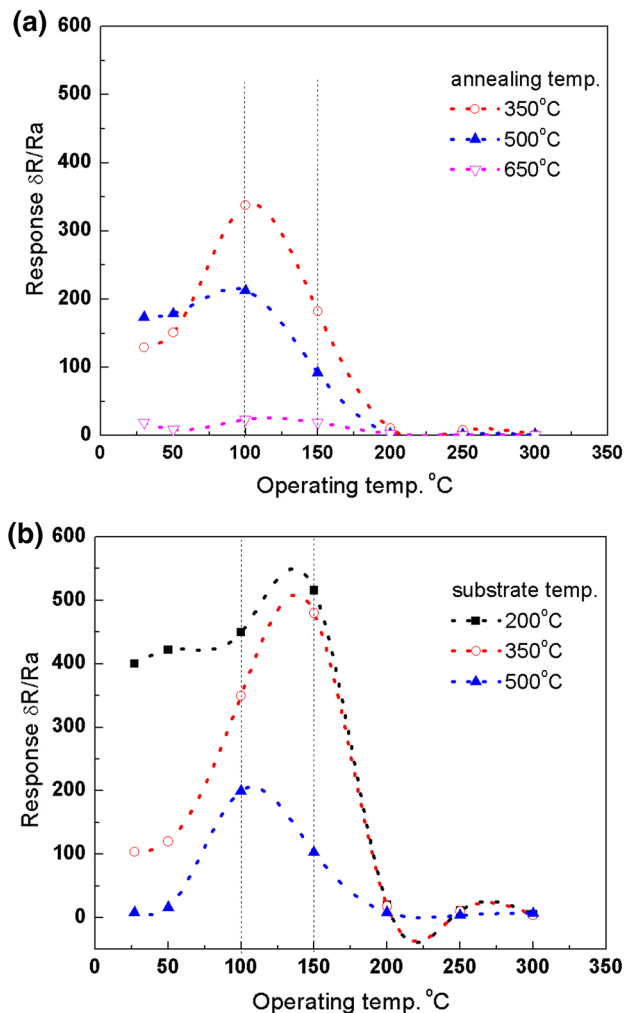
observed for in situ-heated sensors, as shown in Fig. 8b. Interestingly, the response peak was shifted to lower operating temperature of 100 °C for the sensor deposited at a substrate temperature of 500 °C instead of the operating temperature of 150 °C for the sensors deposited at 200 and 350 °C. This might be attributed to the change in grain size, which can lead to a change in both the magnitude and operating temperature of the response peak [35, 36]. The highest responses obtained to 2 ppm NO_2 were 516, 480, and 200 for the sensors deposited at 200, 350, and 500 °C, respectively. Thus, if we consider the operation of present sensors at low temperatures, such as RT or 50 °C, the in situ-heated sensor is highly sensitive for NO_2 gas and thus consumes a low energy because of its low operating temperature. If we consider the sensor to be operated with the highest response, the in situ-heated sensor has a good performance and response to energy consumption slightly higher than that of post-annealed sensor which has lower response and operating temperature.
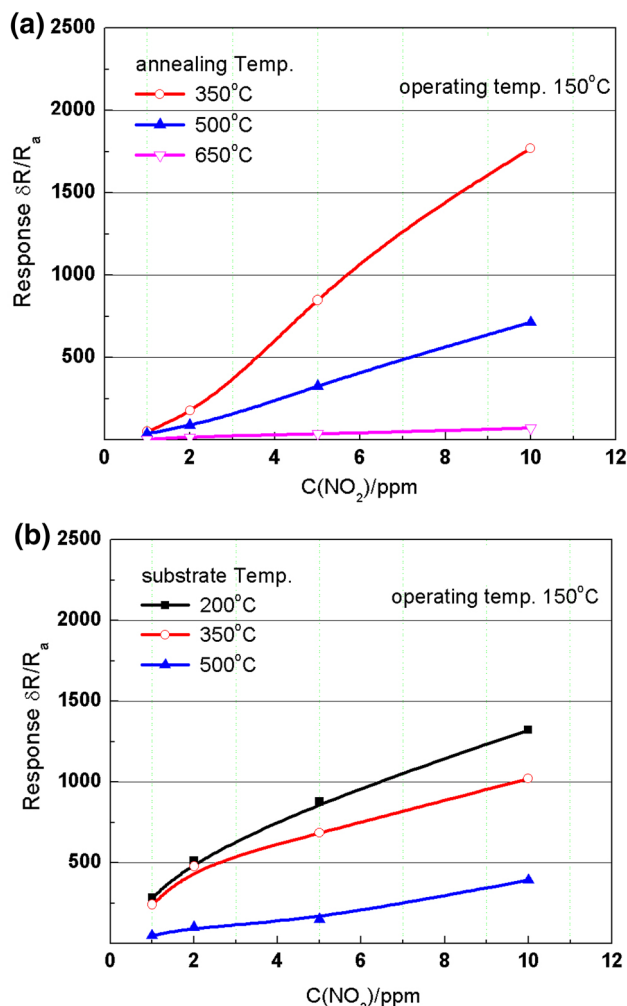
Fig. 9 Response of sensors at various concentrations

It is well known that the oxygen vacancies and oxygen species play a role in determining the electrical transport properties of SnO$_2$ [28, 37]. For SnO$_2$ film sputtered in an ambiance of oxygen, there should be many oxygen species existed inside the film in the form of chemisorption. The chemisorbed oxygen species trap the electrons from the bulk and effectively compensate the oxygen vacancies. With the re-crystallization of SnO$_2$ film upon thermal treatment, these oxygen species are desorbed. The film also undergoes an oxidation process, and consequently the oxygen vacancy density is reduced at high temperatures. Since the oxidation process is not probable at low temperatures, disruption of oxygen species dominated in case of low temperatures and caused an increase in the oxygen vacancy concentration. With further increase in the temperature, oxygen molecules could get sufficient energy to react with the uncoordinated tin atoms and thus the oxygen vacancies could be reduced [38]. In addition to the change in concentration of oxygen vacancies due to the thermal

treatment, the pore volume of the film was also affected. From Figs. 6 and 8, the results are in a harmony and reflect the strong correlation between the total pore volume and the response of sensor. Highly sensitive sensor possesses a high total pore volume, whereas the less sensitive sensor possesses a less value. Figure 9 shows the sensor response to various NO$_2$ concentrations of 1–10 ppm. The response of sensors increased when the sensors were exposed to more concentration of NO$_2$. The in situ-heated sensors are highly sensitive at lower concentrations than the post-annealed sensors. At high concentrations, both the in situ-heated and post-annealed sensors are highly sensitive, and the highest response of 1770 was observed in the post-annealed sensor of 350 °C, indicating the ability of this sensor for receiving a lot of gas concentration because of its high total pore volume. The in situ-heated sensors are superior in detecting and monitoring a low concentration of NO$_2$ gas, whereas the post-annealed sensors are less sensitive at these concentrations although they are highly sensitive at higher concentrations. Generally, the result reflects the good ability and reliability of sensors in detecting various NO$_2$ concentrations.

4 Conclusions

In case of post-deposition temperature, the as-deposited SnO$_2$ film is amorphous and in order to induce structural stability, a thermal treatment is essentially required. The moderate deposition temperature of in situ heating is sufficient to induce partial crystallization in the film. XRD charts of SnO$_2$ film show the same peaks in case of in situ heating or post-annealing. Both of the in situ-heated and post-annealed films are composed of grains and pores, and the grains contact with each other through necks. The grains and the pores grow up when the post-annealing temperature raises, contrasting in the case of in situ heating. The film became dense and the grain boundaries can be lightly seen by SEM where the pores reduced to very small sizes at high temperatures. For deeper understanding the pore size distribution of SnO$_2$ film, the pore size distribution was measured by the physical adsorption–desorption method. The response of sensors upon exposure to 2 ppm concentration of NO$_2$ gas at various operating temperatures is investigated. Both post-annealing and in situ-heating sensors possess similar behavior of operating temperature dependence of sensor response. Interestingly, the response peak was shifted to lower operating temperature of 100 °C for the sensor deposited at a substrate temperature of 500 °C instead of 150 °C for the sensors deposited at 200 and 350 °C. The response of sensors of in situ heating is higher than that of the sensor of post-annealing. The response is fairly good for NO$_2$ gas at

various temperatures and concentrations. The results are in a harmony and reflect the strong correlation between the total pore volume and the response of sensor.

References

1. B. Son, W. Yang, P. Breysse, T. Chung, Y. Lee, Estimation of occupational and nonoccupational nitrogen dioxide exposure for Korean taxi drivers using a microenvironmental model. Environ. Res. **94**, 291–296 (2004)

2. Bonn, Germany January 2003, Report on a WHO working group, health aspects of air pollution with particulate matter, ozone and nitrogen dioxide, (2003), pp. 1–92

3. S.M. Kanan, O.M. El-Kadri, A.I. Abu-Yousef, M.C. Kanan, Semiconducting metal oxide based sensors for selective gas pollutant detection. Sensors **9**(10), 8158–8196 (2009)

4. G. Sberveglieri, S. Groppelli, P. Nelli, Highly sensitive and selective NOx and NO_2 sensor based on Cd-doped SnO_2 thin films. Sens. Actuators B **4**, 457–461 (1991)

5. G. Williams, G.S.V. Coles, NOx response of tin dioxide based gas sensors. Sens. Actuators B **16**, 349–353 (1993)

6. G. Sberveglieri, G. Faglia, S. Groppelli, P. Nelli, Methods for the preparation of NO, NO_2 and H_2 sensors based on tin oxide thin films, grown by means of the r.f. magnetron sputtering technique. Sens. Actuators B **8**, 79–88 (1992)

7. G. Faglia, P. Nelli, G. Sberveglieri, Frequency effect on highly sensitive NO_2 sensors based on RGTO SnO_2(Al) thin films. Sens. Actuators B **19**, 497–499 (1994)

8. G. Leo, R. Rella, P. Siciliano, S. Capone, J.C. Alonso, V. Pankov, A. Ortiz, Sprayed SnO_2 thin films for NO_2 sensors. Sens. Actuators B **58**, 370–374 (1999)

9. I. Hwang, S. Kim, J. Choi, J. Choi, H. Ji, G. Kim, G. Cao, J. Lee, Synthesis and gas sensing characteristics of highly crystalline ZnO–SnO_2 core–shell nanowires. Sens. Actuators B **148**, 595–600 (2010)

10. N. Yamazoe, New approaches for improving semiconductor gas sensors. Sens. Actuators B **5**, 7–19 (1991)

11. A. Kolmakov, M. Moskovits, Chemical sensing and catalysis by one-dimensional metal-oxide nanostructures. Annu. Rev. Mater. Res. **34**, 151–180 (2004)

12. A. Sharma, M. Tomar, V. Gupta, Low temperature operating SnO_2 thin film sensor loaded with WO_3 micro-discs with enhanced response for NO_2 gas. Sens. Actuators B **161**, 1114–1118 (2012)

13. J. Tamaki, J. Niimi, S. Ogura, S. Konishi, Effect of micro-gap electrode on sensing properties of dilute chlorine gas of indium oxide thin film microsensors. Sens. Actuators B **117**, 353–358 (2006)

14. N.M. Shaalan, T. Yamazaki, T. Kikuta, Effect of micro-electrode geometry on NO_2 gas-sensing characteristics of one-dimensional tin dioxide nanostructure microsensors. Sens. Actuators B **156**, 784–790 (2011)

15. A. Ylinampa, V. Lantto, S. Leppavuori, Some differences between Au and Pt electrodes in SnO_2 thick-film gas sensors. Sens. Actuators B **14**, 602–604 (1993)

16. T. Minami, Transparent conducting oxide semiconductors for transparent electrodes. Semicond. Sci. Technol. **20**, S35–S44 (2005)

17. S.S. Lekshmya, G.P. Daniel, K. Joy, Microstructure and physical properties of sol gel derived SnO_2: Sb thin films for optoelectronic applications. Appl. Surf. Sci. **274**, 95–100 (2013)

18. Z. Jie, H. Li-Hua, G. Shan, Z. Hui, Z. Jing-Gui, Alcohols and acetone sensing properties of SnO_2 thin films deposited by dip-coating. Sens. Actuators B **115**, 460–464 (2006)

19. B. Wei, M. Hsu, P. Su, H. Lin, R. Wu, H. Lai, A novel SnO_2 gas sensor doped with carbon nanotubes operating at room temperature. Sens. Actuators B **101**, 81–89 (2004)

20. L. Francioso, A. Forleo, S. Capone, M. Epifani, A.M. Taurino, P. Siciliano, Nanostructured In_2O_3–SnO_2 sol–gel thin film as material for NO_2 detection. Sens. Actuators B **114**, 646–655 (2006)

21. V. Bilgin, S. Kose, F. Atay, I. Akyuz, The effect of Zn concentration on some physical properties of tin oxide films obtained by ultrasonic spray pyrolysis. Mater. Lett. **58**, 3686–3693 (2004)

22. R.Y. Korotkov, P. Ricou, A.J.E. Farran, Preferred orientations in polycrystalline SnO_2 films grown by atmospheric pressure chemical vapor deposition. Thin Solid Films **502**, 79–87 (2006)

23. A.M. Serventi, R. Dolbec, M.A. El Khakani, R.G. Saint-Jacques, D.G. Rickerby, High-resolution transmission electron microscopy investigation of the nanostructure of undoped and Pt-doped nanocrystalline pulsed laser deposited SnO_2 thin films. J. Phys. Chem. Solids **64**, 2097–2103 (2003)

24. A.S. Reddy, N.M. Figueiredo, A. Cavaleiro, Nanocrystalline Au:Ag:SnO_2 films prepared by pulsed magnetron sputtering. J. Phys. Chem. Solids **74**, 825–829 (2013)

25. G. Korotcenkov, The role of morphology and crystallographic structure of metal oxides in response of conductometric-type, gas sensors. Mater. Sci. Eng. R **61**, 1–39 (2008)

26. M. Hayashi, T. Hyodo, Y. Shimizu, M. Egashira, Effect of microstructure of mesoporous SnO_2 powders on their H_2 sensing properties. Sens. Actuators B **141**, 465–470 (2009)

27. H. Ahn, J.H. Noh, S. Kim, R.A. Overfelt, Y.S. Yoon, D. Kim, Effect of annealing and argon-to-oxygen ration on sputtered SnO_2 thin film sensor for ethylene gas detection. Mater. Chem. Phys. **124**, 563–568 (2010)

28. B. Ruhland, T. Becker, G. Muller, Gas-kinetic interactions of nitrous oxides with SnO_2 surfaces. Sens. Actuators B **50**, 85–94 (1998)

29. A. Sharma, M. Tomar, V. Gupta, SnO_2 thin film sensor with enhanced response for NO_2 gas at lower temperatures. Sens. Actuators B **156**, 743–752 (2011)

30. Y. Shen, T. Yamazaki, Z. Liu, C. Jin, T. Kikuta, N. Nakatani, Porous SnO_2 sputtered films with high H_2 sensitivity at low operation temperature. Thin Solid Films **516**, 5111–5117 (2008)

31. T. Yamazaki, T. Furuta, Y. Shen, C. Jin, T. Kikuta, N. Nakatani, Effective surface area of SnO_2 sputtered films evaluated by measurement of physical adsorption isotherms. Jpn. J. Appl. Phys. **45**, 9180–9184 (2006)

32. K.S.W. Sing, D.H. Everett, R.A.W. Haul, L. Moscou, R.A. Pierotti, J. Rouquerol, T. Siemieniewska, "Reporting physisorption data for gas/solid systems" with special reference to the determination of surface area and porosity. Pure Appl. Chem. **57**, 603–619 (1985)

33. J. Pelleg, G. Sade, M. Sinder, D. Mogilyanski, Compositional and structural changes in TiB_2 films induced by bias, in situ and post-deposition annealing, respectively. Phys. B **381**, 118–127 (2006)

34. Z. Liu, T. Yamazaki, Y. Shen, T. Kikuta, N. Nakatani, Influence of annealing on microstructure and NO_2-sensing properties of sputtered WO_3 thin Films. Sens. Actuators B **128**, 173–178 (2007)

35. G. Korotcenkov, V. Brinzari, J. Schwank, A. Cerneavschi, Possibilities of aerosol technology for deposition of SnO_2-based films with improved gas sensing characteristics. Mater. Sci. Eng. C **19**, 73–77 (2002)

36. N.M. Shaalan, T. Yamazaki, T. Kikuta, Influence of morphology and structure geometry on NO_2 gas-sensing characteristics of

SnO$_2$ nanostructures synthesized via a thermal evaporation method. Sens. Actuators B **153**, 11–16 (2011)

37. C. Ke, W. Zhu, J.S. Pan, Z. Yang, Annealing temperature dependent oxygen vacancy behavior in SnO$_2$ thin films fabricated by pulsed laser deposition. Curr. Appl. Phys. **11**, S306–S309 (2011)

38. A.F. Khan, M. Mehmood, A.M. Bhatti, Effect of annealing on electrical resistivity of rf-magnetron sputtered nanostructured SnO$_2$ thin film. Appl. Surf. Sci. **255**, 8562–8565 (2009)